A group-theoretical approach to enumerating magnetoelectric and multiferroic couplings in perovskites

Mark S. Senn[a]* and Nicholas C. Bristowe[b,c]

[a]Department of Chemistry, University of Warwick, Gibbet Hill, Coventry, CV4 7AL, UK, [b]School of Physical Sciences, University of Kent, Canterbury CT2 7NH, UK, and [c]Department of Materials, Imperial College London, London SW7 2AZ, UK. *Correspondence e-mail: m.senn@warwick.ac.uk

A group-theoretical approach is used to enumerate the possible couplings between magnetism and ferroelectric polarization in the parent $Pm\bar{3}m$ perovskite structure. It is shown that third-order magnetoelectric coupling terms must always involve magnetic ordering at the A and B sites which either transforms both as R-point or both as X-point time-odd irreducible representations (irreps). For fourth-order couplings it is demonstrated that this criterion may be relaxed allowing couplings involving irreps at X-, M- and R-points which collectively conserve crystal momentum, producing a magneto-electric effect arising from only B-site magnetic order. In this case, exactly two of the three irreps entering the order parameter must be time-odd irreps and either one or all must be odd with respect to inversion symmetry. It is possible to show that the time-even irreps in this triad must transform as one of: X_1^+, $M_{3,5}^-$ or R_5^+, corresponding to A-site cation order, A-site antipolar displacements or anion rocksalt ordering, respectively. This greatly reduces the search space for type-II multiferroic perovskites. Similar arguments are used to demonstrate how weak ferromagnetism may be engineered and a variety of schemes are proposed for coupling this to ferroelectric polarization. The approach is illustrated with density functional theory calculations on magnetoelectric couplings and, by considering the literature, suggestions are given of which avenues of research are likely to be most promising in the design of novel magnetoelectric materials.

1. Introduction

The classification of distortions in functional materials is an important part of the process of understanding the structure–property relationship. Perovskites (ABX_3) are among the most studied systems, which is in part due to the many functional properties that they exhibit, but also due to their richness in structural distortions and phase transitions. Schemes classifying the ubiquitous rotations and tilts of the quasi-rigid BO_6 octahedra that drive many of these phase transitions in perovskites can be conveniently classified in terms of Glazer notation (Glazer, 1972), and other such schemes also exist for classifying distortions in layered perovskite such as Ruddlesden–Poppers (Aleksandrov & Bartolome, 1994). While these schemes have enjoyed much success due to their intuitive nature, there are several limitations, in particular that they are not easily generalized to different systems. Even within the perovskite family, with additional symmetry breaking with respect to the ABX_3 aristotype, it is no longer clear how the occurrence of tilts and rotations can be unambiguously described, or indeed how the symmetry lowering implied by the combined orderings can be derived.

More formally, the degrees of freedom in an aristotype 'parent' structure, such as the $Pm\bar{3}m$ ABX_3 perovskite, may be
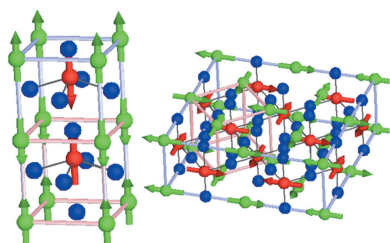
defined as transforming as irreducible representations (irreps) of the parent space group (and setting). The irreps for all special positions in reciprocal space have been tabulated by various authors including by Bradley & Cracknell (1972), Miller & Love (1967), Kovalev (1993) and more recently also at non-special k-points (Stokes *et al.*, 2013). With knowledge of these irreps, it is possible to compute the isotropy subgroups of the 230 space groups (Stokes & Hatch, 1988), which are the subgroups accessible due to the action of an order parameter (OP) transforming as one of these irreps.

Online tools such as *ISODISTORT* (Campbell *et al.*, 2006) and *AMPLIMODES* on the Bilbao Crystallographic Server (Aroyo *et al.*, 2006; Orobengoa *et al.*, 2009) allow distorted structures to be easily decomposed in terms of irreps of a parent space group, and it is now possible to superpose up to three irreps with associated independent incommensurate propagation vectors, and derive the possible subgroups and secondary order parameters (SOPs) (Stokes & Campbell, 2017). Additionally, these programs now generate outputs that can be directly read by Rietveld and single-crystal refinement programs (Campbell *et al.*, 2007; Perez-Mato *et al.*, 2010), allowing refinements to be performed in a symmetry-adapted basis and facilitating easy identification of the active order parameters in a given phase transition.

As a result of much of this work, several group-theoretical studies have emerged that have more formally classified distortions in perovskite-related materials. These include group-theoretical analysis of octahedral tilting in perovskites (Howard & Stokes, 1998, 2005; Knight, 2009), cation-ordered and Jahn–Teller distortions in perovskites (Howard & Carpenter, 2010), ferroelectric perovskites (Stokes *et al.*, 2002), anion ordering (Talanov *et al.*, 2016), and works on layered Ruddlesden–Poppers (Hatch & Stokes, 1987; Hatch *et al.*, 1989). One particularly valuable aspect of classifying these distortions in the formal language of irreps is to understand physical phenomena that can arise due to secondary order parameters which feature at linear order in the Landau-style free energy potential. These odd order terms may always adopt a sign such that they act to lower the overall free energy and hence symmetry analysis alone is sufficient to identify their instability. The process of ascertaining these couplings is greatly simplified using the ideas of invariants analysis (Stokes & Hatch, 1991; Saxena *et al.*, 1994) when constructing the Landau-style free energy expansion about the parent undistorted phase, and online tools for doing this also exist (Hatch & Stokes, 2003).

This process is particularly valuable when understanding improper ferroelectricity (Levanyuk & Sannikov, 1974) where third-order terms in the free energy expansion are invariably the key to understanding the resulting polarization. This area has enjoyed a renaissance in the form of the recently much discussed 'hybrid improper ferroelectric' mechanism [*e.g.* see Benedek *et al.* (2015) for a recent review]. The powerful use of magnetic superspace groups for describing multiferroic materials has also allowed magnetoelectric couplings to be trivially identified through analysis of secondary order parameters (Perez-Mato *et al.*, 2012). Antisymmetric exchange

arguments with respect to the parent perovskite structure have also been used to explain the dominant anisotropic terms that control the directions of spin ordering (Khalyavin *et al.*, 2015). And of course, the occurrence of weak ferromagnetism (wFM) by the Dzyaloshinsky–Moriya (DM) interaction (Dzyaloshinsky, 1958; Moriya, 1960) was first originally rationalized based on such symmetry arguments alone (Dzyaloshinsky, 1958).

Using many of the ideas above, and with the aid of the *ISODISTORT* (Campbell *et al.*, 2006) tool, we seek here to generalize a recipe for inducing magnetoelectricity in the parent $Pm\bar{3}m$ perovskite. These recipes are based on symmetry arguments alone, and we use as the ingredients structural and magnetic degrees of freedom, which we classify in terms of transforming as irreps of the parent space group. Our results clearly show why certain kinds of coupled distortions and magnetic ordering can never lead to ferroelectric or ferromagnetic secondary order parameters, and by considering which orderings and cation arrangements are commonly observed, we are able to identify several promising avenues for further investigation.

The article is arranged as follows. In §2, we first classify the ingredients for symmetry breaking that are at our disposal in terms of irreps of the parent $Pm\bar{3}m$ space group. To keep our results as general as possible, we will also describe cation and anion ordering in terms of irreps, rather than forming new parent space groups. We then proceed to give various recipes for achieving (multi)ferroic orderings as a consequence of different symmetry-breaking distortions. In §3, for completeness we give the recipe for (hybrid) improper ferroelectricity, while in §§4, 5, 6 we discuss magnetoelectric couplings arising due to third- and fourth-order terms in the free energy expansion. As the most useful multiferroics are those that are ferromagnets (rather than antiferromagnets), in §7 we explain how similar ideas can be used to design systems that exhibit wFM. We also consider in this section systems in which either polarization (P) or wFM is supplied as an external order parameter (as a magnetic or electric field) resulting in the development of wFM or P, respectively, in response to the stimuli. Finally, in §8 we put all of our above ideas together and deal with the design of materials that are both wFM and ferroelectric, and have indirect coupling through at least one primary order parameter (POP).

2. Ingredients for symmetry breaking

First we classify the magnetic degrees of freedom at our disposal in terms of irreps of the space group $Pm\bar{3}m$. We classify all of these in terms of irreps of the parent perovskite structure $Pm\bar{3}m$ with setting A $1a$ $(0, 0, 0)$; B $1b$ $(\frac{1}{2}, \frac{1}{2}, \frac{1}{2})$; X $3c$ $(0, \frac{1}{2}, \frac{1}{2})$. We note that reversing the setting of the structure will result in many of the irrep labels changing, in particular at the X- and R-points, irreps labelled as '+' will correspond to another numbered irrep with the '−' sign and *vice versa*. The origin of this is that the sign part in these irrep labels refers to whether or not parity (with respect to inversion symmetry) is conserved or violated at the origin $(0, 0, 0)$, and hence inter-

Table 1
Ingredients for symmetry breaking in the perovskite structure, classified in terms of transforming as irreps of the parent perovskite structure, with the *A* site at the origin (the corresponding irrep labels for the setting with the *B* site at the origin are given in parentheses).

Ingredient	Γ	X	M	R
Strain	Γ_3^+; Γ_5^+			
Cation order (*A*)		X_1^+ (X_3^-)	M_1^+ (M_4^+)	R_1^+ (R_2^-)
Cation order (*B*)		X_3^- (X_1^+)	M_4^+ (M_1^+)	R_2^- (R_1^+)
Anion order (O)		X_1^+ (X_3^-)	M_4^+ (M_1^+); M_5^- (M_5^-)	R_5^+ (R_4^-)
(Anti-)Polar (*A*)	Γ_4^-	X_3^- (X_1^+); X_5^- (X_5^+)	M_3^- (M_2^-); M_5^- (M_5^-)	R_4^- (R_5^+)
(Anti-)Polar (*B*)	Γ_4^-	X_1^+ (X_3^-); X_5^- (X_5^-)	M_2^- (M_3^-); M_5^- (M_5^-)	R_5^+ (R_4^-)
Jahn–Teller modes	Γ_3^+	X_3^- (X_1^+)	M_3^+ (M_2^+)	R_3^- (R_3^+)
Octahedral tilt modes			M_2^+ (M_3^+)	R_5^- (R_4^+)
Magnetic order (*A*)	$m\Gamma_3^+$	mX_3^+ (mX_1^-); mX_5^+ (mX_5^-)	mM_3^+ (mM_2^+); mM_5^+ (mM_5^+)	mR_4^+ (mR_5^-)
Magnetic order (*B*)	$m\Gamma_4^+$	mX_1^- (mX_3^+); mX_5^- (mX_5^+)	mM_2^+ (mM_3^+); mM_5^+ (mM_5^+)	mR_5^- (mR_4^+)

changing the atom at the origin naturally affects the distortions physically being described by a particular representation. The orderings of the magnetic degrees of freedom will ultimately be devised in such a way as to drive secondary order parameters that are related to ferroelectricity. We restrict ourselves here to the basic types of antiferromagnetic ordering which are commonly observed in perovskites. These are often characterized as A, C and G type having one, two and three antiferromagnetic (AFM) nodes, respectively. They may be classified as corresponding to orderings which transform as irreps at the $X[0, \frac{1}{2}, 0]$-, $M[\frac{1}{2}, \frac{1}{2}, 0]$- and $R[\frac{1}{2}, \frac{1}{2}, \frac{1}{2}]$-points (Fig. 1). It is important to note that magnetic structures such as A_x and A_{yz}, which correspond to an ordering with propagation vector $X[\frac{1}{2}, 0, 0]$ with moment along the propagation axis and

perpendicular to it, transform as distinct irreps in this analysis, and will imply physically distinct secondary order parameters. This forms the basis of the antisymmetric exchange arguments of Khalyavin *et al.* (2015) to determine spin (exchange) anisotropy, and this is why this analysis is so powerful in the perovskite structure where the magnetic atoms sit on high-symmetry sites. Fig. 1 gives full details of how the spin arrangements are related to irreps.

Next we classify the various structural degrees of freedom within the perovskite structure for inducing symmetry-lowering phase transitions. The ingredients at our disposal are the commonly observed octahedral rotation and tilt modes, Jahn–Teller distortion modes, cation (charge) ordering modes, antipolar modes and strain. These are all listed in Table 1, along with their corresponding labels in the alternative setting [*A* at $(\frac{1}{2}, \frac{1}{2}, \frac{1}{2})$]. Some of these degrees of freedom will be accessible *via* physical control parameters (such as application of epitaxial strain) whilst others only by chemical design (for example, by inclusion of Jahn–Teller active cations). In the analysis, we will also classify cation and anion orderings in the perovskite structure in terms of transforming as irreps of the parent perovskite. For example, rocksalt cation ordering at the *B* site transforms as R_2^- and *A*-site layered cation order as X_1^+. We may even classify the highly distorted cation-ordered $A'A_3B_4O_{12}$ quadruple perovskite with aristotype $Im\bar{3}$ as having cation orderings transform as M_1^+ [with three *k*-actives $= (\frac{1}{2}, \frac{1}{2}, 0); (0, \frac{1}{2}, \frac{1}{2}); (\frac{1}{2}, 0, \frac{1}{2})$] and octahedral rotations that stabilize the A' square-planar coordination transforming as M_2^+.

Finally, the desired property, ferroelectricity, transforms as the polar mode belonging to the irrep Γ_4^-. Γ_4^- is a three-dimensional irrep; the most general order parameter direction (OPD) associated with this would hence be written as OP(*a*,*b*,*c*), where special directions (*a*, 0, 0), (*a*, *a*, 0) and (*a*, *a*, *a*) correspond to tetragonal, orthorhombic and rhombohedral directions, respectively, for the macroscopic polarization and off-centre displacements of the atoms. For a full discussion of notation relating to OPDs, including cases where multiple irreps enter into the OP, as will become pertinent in future discussion, the reader is directed to Appendix A. Please note that throughout this article we choose to list the full OPD, instead of the space group and setting. The two are equivalent, but we choose the OPD for the sake of brevity, and also due to
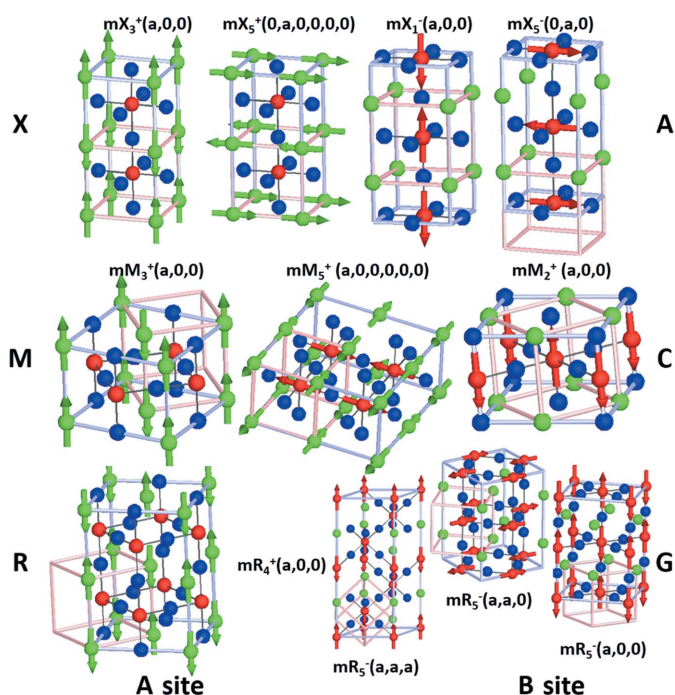

Figure 1
Basic AFM magnetic orderings of the perovskite structure with associated irrep labels and illustrated along high-symmetry OPD *A* sites, *B* sites and *X* sites are shown as green, red and blue spheres, respectively. The parent cubic unit cell is shown in pink so as to illustrate the relationship with the new crystallographic axes (grey). All figures are drawn in *ISODISTORT*.

its descriptive nature with respect to the magnetic and structural orderings that are allowed to occur. We will now discuss the general design principles by which we can combine the aforementioned degrees of freedom to produce Γ_4^- as a secondary OP.

3. Recipes for improper ferroelectric couplings

We begin by considering structural irreps (transforming as time-even) alone, and how they may combine to produce improper ferroelectric couplings, before considering couplings with magnetic irreps in the next section. The concept of improper ferroelectricity was first introduced several decades ago by Levanyuk & Sannikov (1974), but recently there has been renewed interest [see reviews (Varignon *et al.*, 2015*b*; Benedek *et al.*, 2015; Young *et al.*, 2015)] after its observation in epitaxially grown layered perovskite systems (Bousquet *et al.*, 2008). In light of work that has highlighted the existence of improper ferroelectricity in naturally layered perovskite-like Ruddlesden–Popper systems (Benedek & Fennie, 2011), we believe it is also of interest to enumerate all such possible couplings in the aristotypical perovskite structure here, at least to illustrate the idea, introduce the topic and review the literature, before moving on to magnetoelectric couplings.

The general recipe for constructing improper ferroelectric coupling terms in the Landau-style free energy expansion about the parent perovskite structure that we will use is as follows. The principle of invariants analysis (Hatch & Stokes, 2003) means that, at each term in the free energy expansion, crystal momentum and inversion symmetry must be conserved. In the next section we also consider magnetism, when the additional constraint of time reversal symmetry must be conserved.

We seek initially the dominant coupling term, which means that we should consider the lowest-order term in the free energy expansion that is achievable which has linear order in P. We restrict ourselves to coupling terms only of linear order in P since in these cases we can be sure that symmetry analysis can be sufficient to infer the appearance of P, unlike in even orders where calculation of the sign and strength of the coefficients would be necessary. For example, since P transforms as inversion-odd and has zero crystal momentum, the lowest-order term will be third order (ABP), which has been termed hybrid improper ferroelectricity (Bousquet *et al.*, 2008; Benedek & Fennie, 2011; Fukushima *et al.*, 2011). Since trilinear terms will always act to lower the free energy, if A and B are unstable, then P will also be present, adopting a sign (direction of polarization) such as to stabilize the overall free energy.

Invariants analysis tells us that:

for P is inversion-odd; [P] = [0, 0, 0].[1]

A·B is inversion-odd; [A] + [B] = [0, 0, 0] must be obeyed leading to all quantities being conserved in the trilinear term:

A·B·P is inversion-even; [A] + [B] + [P] = [0, 0, 0] to be true, where [A] represents crystal momentum associated with OP A and A·B is the multiplication of the characters of the irreps associated with the OP A and B.[2]

One may further convince oneself that A $\neq$ B must be true for this condition to be fulfilled for otherwise AB would be inversion-even, meaning that the quadratic linear term A^2P is not permissible in the free energy expansion, and so is not a term that can drive an improper coupling.[3] In summary we can say that A and B must both be of opposite parity with respect to inversion symmetry and must have equal crystal momentum. We will explore all trilinear couplings possible within the perovskite parent structure for OPs transforming as X-, M- and R-point irreps below.

The above criterion is necessary, but in a few cases not always sufficient to ensure the desired improper ferroelectric coupling. In practice, this may be conveniently checked using 'Method 2' of the online tool *ISODISTORT* where multiple irreps may be superimposed to form the primary OP of the parent perovskite structure. The program then lists all the possible OPDs associated with this, along with the resulting secondary OPs and the space-group symmetry and basis with respect to the parent structure. It is then trivial to identify from either the space group or the list of secondary OPs if an improper ferroelectric coupling will occur.

Any of the following that have atomic displacements that transform collectively as these irreps will feature in a trilinear term with Γ_4^- (where $\oplus$ represents the direct sum):

$$X_{1,2,3}^+ \oplus X_{3,5}^-$$

$$M_{1,2,3,4,5}^+ \oplus M_{2,3,5}^-$$

$$R_{1,5}^+ \oplus R_{2,3,4,5}^-$$

While many of these may be difficult to achieve in practice, there are several promising candidates. For example, columnar *A*-site cation order (M_1^+) with antipolar *B*-site displacements (M_5^-) can lead to a trilinear term $M_1^+ M_5^- \Gamma_4^-$. We believe this could be the cause of the ferroelectric polarization recently reported in high-pressure perovskite $CaMnTi_2O_6$ (Aimi *et al.*, 2014). Indeed, cation or anion ordering at any of the perovskite sites at the M-point along with antipolar distortions at the *A* or *B* sites would produce an improper ferroelectric polarization. In-phase tilting (M_2^+) or the M-point Jahn–Teller mode (M_3^+) can alternatively be used in conjunction with the antipolar displacements (such as M_5^-) to induce a polarization, which has been recently predicted in the *Pmc*2$_1$ phase of several perovskites (Yang *et al.*, 2012, 2014; Varignon *et al.*,

---

[1] In general the inversion symmetry breaking distortion will transform as the polar Γ_4^- mode; however sometimes the symmetry breaking will instead be associated with another Γ^- mode which is piezoelectric in nature.

[2] Strictly speaking, the relevant OPs are vectors whose elements (real or imaginary numbers) reflect the amplitude of the atomic displacements or magnetic moments that transform according to specific irreps. However, since for the purposes of our symmetry analysis, the information we require concerning crystal momentum and parity is encoded in the irrep label (and we are not concerned with amplitude here), we will also label the OPs using this notation.

[3] A^2P terms can be possible in some systems where A transforms as an irrep with imaginary character, but this is not relevant for the zone-boundary irreps of $Pm\bar{3}m$ that we consider here.

2016), and might also be the origin of the (ionic component of the) ferroelectricity in the $P2_1nm$ half-doped manganites (Giovannetti *et al.*, 2009; Rodriguez *et al.*, 2005).

The commonly observed rocksalt cation ordering at the B site (King & Woodward, 2010) along with (R-point) antipolar distortions on the A site will also produce an improper ferroelectric coupling. While the former is commonly observed, controlling the periodicity of the antipolar distortions such as those induced by lone-pair ordering will be challenging. Cation order on the A sites at the R-point (rocksalt) along with octahedral tilt modes would also produce an improper ferroelectric coupling, as recently predicted through first-principles calculations (Young & Rondinelli, 2013). However, it should be noted that A-site cation ordering is more commonly found to be in a layered (X-point) arrangement (King & Woodward, 2010). Very recent reports of improper ferroelectricity in the 134 perovskite $HgMn_3Mn_4O_{12}$ can also be understood with respect to the present symmetry analysis of ABO_3 perovskites (Chen *et al.*, 2018). In this case, the atomic displacements associated with the orbital and charge ordering degrees of freedom on the A and B sites transform as irreps of the parent space group $Pm\bar{3}m$ R_5^+ and R_3^-.

A-site cation layering (X_1^+) in combination with antipolar A-cation motions is indeed sufficient to induce P. Again, whilst the former is fairly common, the latter is only expected to be an unstable lattice distortion for low tolerance factor perovskites (Mulder *et al.*, 2013). However it can itself manifest through an improper appearance with two tilting modes (M_2^+ R_5^- X_5^-), which gives rise to the fourth-order term described below. At the X-point, one other trilinear term has been predicted to play a role in the $P2_1$ phase of strained $CaTiO_3$, whereby A- and B-site antipolar (X_5^+ and X_5^-) motions induce P (Zhou & Rabe, 2013).

Fourth-order terms in P should also be considered and may be more promising on account of the extra degree of flexibility allowed in the recipe.[4] Here, crystal momentum considerations mean that each relevant fourth-order term must take the form:

A·B·C is inversion-odd; [A] + [B] + [C] = [0, 0, 0] must be obeyed leading to all quantities being conserved in the trilinear term:

A·B·C·P is inversion-even; [A] + [B] + [C] + [P] = [0, 0, 0].

One of the most promising fourth-order candidates involves OPs associated with X^+, M^+, R^- and Γ_4^-: for example, A-site layered cation ordering (X_1^+), octahedral tilt mode (M_2^+) and octahedral tilt mode (R_5^-). This explains the significance of layering (X_1^+) in allowing the two octahedral rotation modes to couple together to produce a polarization and has been the most common example of improper ferroelectricity in perovskites as illustrated in both artificially (Bousquet *et al.*, 2008; Rondinelli & Fennie, 2012) and naturally layered double perovskites (Fukushima *et al.*, 2011). A similar term, predicted in half-doped titanates (Bristowe *et al.*, 2015), includes A-site

layered cation ordering (X_1^+), M-point Jahn–Teller (M_3^+) and octahedral tilt modes (R_5^-). Other possibilities include A-site striped cation ordering (X_1^+), tilting (R_5^-) and charge order (M_4^+), which we believe to be the origin of the improper polarization in $SmBaMn_2O_6$ (Yamauchi, 2013). Alternatively Jahn–Teller induced, M_3^+ and R_3^-, ferroelectricity has been discussed in A-site striped cation ordered (X_1^+) rare-earth vanadates (Varignon *et al.*, 2015a). Perhaps an interesting avenue for future research is to use anion ordering since the X_1^+ irrep is also made possible by anion vacancy ordering, which for example is sometimes seen in the cobaltates (Karen *et al.*, 2001; Vogt *et al.*, 2000; Castillo-Martínez *et al.*, 2006).

Other chemically and structurally less promising schemes are still worth a mention: X^- M^- R^- Γ_4^-, for example, striped order at the A site (X), antipolar order at the B site (M) and rocksalt cation order at the B site (R); X^- M^+ R^+ Γ_4^-, striped B-site cation order (X_3^-), octahedral tilt mode (M_2^+), antipolar distortion on the B site (R_5^+); and X^+ M^- R^+ Γ_4^-, A-site striped cation ordering (X_1^+), antipolar distortions on the B site (M_2^-), anion order (R_5^+). Finally, we note that the inclusion of organic cations on the A site or organic link molecules on the X site greatly increases the possible number of such improper ferroelectric coupling schemes (Boström *et al.*, 2018) and provides a promising route for designing novel functional materials.

4. Recipes for magnetoelectric coupling

We can extend the ideas discussed above for improper ferroelectrics to magnetoelectric couplings including time-odd irreps that describe magnetic order. We seek initially the strongest magnetoelectric coupling term possible: this means that as before we should consider the lowest-order term in the free energy expansion that is achievable. Since P transforms as time-even, inversion-odd and has zero crystal momentum, the lowest-order term involving two zone-boundary irreps will be third order (ABP). Invariants analysis tells us that:

for P is time-even; P is inversion-odd; [P] = [0, 0, 0].

A·B is time-even; A·B is inversion-odd; [A] + [B] = [0, 0, 0] must be obeyed leading to all quantities being conserved in the trilinear term:

A·B·P is time-even; A·B·P is inversion-even; [A] + [B] + [P] = [0, 0, 0].

As we are seeking a magnetoelectric coupling, at least one of A or B must be magnetic, and inspection of the condition that A·B is time-even means that therefore both A and B must transform as a time-odd irrep. One may further convince oneself that A ≠ B must be true for this condition to be fulfilled for otherwise AB would be inversion-even, meaning that the quadratic linear term A^2P is not permissible in the free energy expansion, and so is not a term that can drive an electromagnetic coupling.[5] Taking everything together we can say that A and B must both be time-odd, of opposite parity

---

[4] Although we consider these formally as fourth-order terms here we emphasize that they might equally be third-order terms of a lower-symmetry perovskite structure that has already undergone some cation ordering or other structural distortion.

[5] A^2P terms can be possible in some systems where A transforms as an irrep with imaginary character, but this is not relevant for the zone-boundary irreps of $Pm\bar{3}m$ that we consider here.

with respect to inversion symmetry and must have equal crystal momentum.

As before with the improper ferroelectrics, the list of magnetoelectric trilinear coupling terms (with respect to the perovskite parent structure) will prove to be rather restrictive, and so we will also consider fourth-order terms in the free energy expansion. This would be equivalent to considering trilinear terms of a new parent structure which has one of the many reported subgroups of $Pm\bar{3}m$ due to structural distortions or cation orderings, which themselves can be classified as transforming as irreps of $Pm\bar{3}m$. However, from a materials design perspective, it is most convenient to always list these couplings with respect to the aristotypical symmetry.

If we consider couplings at the fourth order we may now construct terms as follows from the three primary OPs (A, B and C):

A·B·C is time-even

A·B·C is inversion-odd

[A] + [B] + [C] = [0, 0, 0].

If we are seeking a magnetoelectric coupling, precisely two of these terms must be time-odd (since P will always be time-even), but the constraint that the sum of these two terms must conserve crystal momentum is now lifted. We will refer to this design approach as 'closing the momentum triangle', since now three irreps may be chosen to produce zero crystal momentum transfer.

This gives greater flexibility in the design strategy, but the price of course is that now three primary OPs are required. This means either these must all spontaneously become thermodynamically favourable at the phase transition, or more likely, and as discussed above, the structure will already contain distortions to the parent phase (such as octahedral rotations) which are ubiquitous in the perovskite structure.

Our approach outlined above is similar in spirit in some ways to that used to consider possible magnetoelectric couplings in the incommensurate phase of BaMnF$_4$ (Fox et $al.$, 1980). However, our approach differs in that we perform the Landau-style expansion of the free energy about a hypothetical aristotypical symmetry, rather than the experimentally observed high-temperature phases. The benefit of our approach is that it encodes as much information as possible regarding the crystal momentum and parity of the time-odd and -even OPs into the problem, making it particularly easy to predict magnetoelectric couplings based on symmetry arguments alone, as we demonstrate here.

5. Trilinear magnetoelectric couplings in AFM systems

We start from the criteria derived above which means that we may superpose the following time-odd irreps when constructing the OP:

$$mR_4^+ \oplus mR_5^- \; ; \; mX_3^+ \oplus mX_1^- \; ; \; mX_5^+ \oplus mX_5^- \; .$$

At the M-point, all possible magnetic orderings transform as mM$^+$ and so no magnetoelectric couplings are possible. This finding immediately rules out a large area of search space. Furthermore, magnetic moments on the A-site cations trans-

form always as mX$^+$ and mR$^+$ and on the B site always as mX$^-$ and mR$^-$, meaning any such trilinear magnetoelectric coupling mechanism must involve order on both A and B sites simultaneously. We take these three possible couplings in turn now, and consider which are the most physical and if any experimental realizations already exist.

For $mX_3^+ \oplus mX_1^-$, the OP is six dimensional OP(a;b;c|d;e;f) and the different choices of OPD result in a total of 22 possible isotropy subgroups. Only a subset of these, in which the condition for conserving crystal momentum is satisfied at a linear term in polarization, have broken inversion symmetry. While many of these lead to polar space groups, some only result in piezoelectric couplings. In these cases application of strain (either external or internal from ferroelastic distortions) will produce the desired polar ground state. Those with broken inversion symmetry correspond to OPDs of OP(a;0;0|d;0;0), OP(a;0;a|d;0;d), OP(a;$\bar{a}$;a|d;$\bar{d}$;d) (see Fig. 2). Of these only OP(a;0;0|d;0;0) represents a single k-active and collinear solution, and we shall focus on this for the rest of our discussion. The isotropy group is P_c4cc with basis = [(1, 0, 0),(0, 0, 1),(0, −2, 0)] + (0, 0, 0) and SOPs Γ_4^- (polar mode) and Γ_3^+ (tetragonal strain). This OPD corresponds to the magnetic moments aligned parallel to the propagation vector on both A and B sites.

To illustrate that our symmetry arguments can be used to identify improper ferroelectric couplings, we perform the following computational experiment. Density functional theory (DFT) calculations using the $VASP$ code (Kresse & Hafner, 1993; Kresse & Furthmüller, 1996) (version 5.4.1) were executed on a hypothetical cubic GdFeO$_3$ structure in which the unit-cell parameter (the only degree of freedom) was fixed at a = 3.65 Å. This contracted unit cell was to ensure that no polar instability existed in the phonon dispersion curve [in the ferromagnetic (FM) state, or with spin–orbit coupling turned off], such that any later appearance of Γ_4^- (with spin–orbit coupling turned on) could be identified as arising through improper, rather than proper, ferroelectricity. This is illustrated in Fig. 3 where the polar mode [Γ_4^- OP (0, h, 0)] is condensed with different amplitudes in the FM phase (mΓ_4^+) to give the expected single well potential centred at zero.

We used the GGA PBEsol exchange correlation functional (Perdew et $al.$, 2008) and PAW pseudopotentials (PBE func-
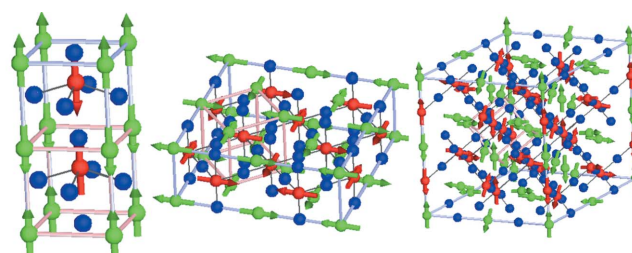
X$_3^+$X$_1^-$(a,0,0|b,0,0) P$_c$4cc   X$_3^+$X$_1^-$(a,0,a|b,0,b) A$_b$bm2   X$_3^+$X$_1^-$(a,-a,a|b,-b,b) R$_I$3c

Figure 2
Magnetic structures giving rise to the magnetoelectric effect resulting from the action of the OP(a,b,c|d,e,f) transforming as mX$_3^+$ ⊕ mX$_1^-$, shown along the high-symmetry directions OP(a,0,0|d,0,0), OP(a,a,0|d,d,0), OP(a,$\bar{a}$,a|d,$\bar{d}$,d).

tional, version 5.2) with the following valence electron configurations: $5s^2 5p^6 6s^2 4f^8$ (Gd), $3p^6 4s^2 3d^6$ (Fe) and $2s^2 2p^4$ (O). An on-site Coulomb repulsion U (Liechtenstein *et al.*, 1995) was taken as 4 ev for the Gd f electrons and 8 ev for the Fe $3d$ electrons, which further stiffened Γ_4^-, whilst keeping the system insulating. A planewave cut-off of 900 eV and a $6 \times 6 \times 6$ k-grid with respect to the cubic cell were employed.

We then repeat these calculations with magnetic moments fixed on the A and B sites that transform according to the irreps mX_3^+ and mX_1^- [OP(a,0,0|d,0,0)]. As evident in Fig. 3, the potential shifts away from having a minimum at zero (dashed line) prior to the magnetic interactions being switched on to a position where the minimum energy is at a finite value of the polar mode. This linear trend of the energy at the origin (inset Fig. 3) is indicative of an improper ferroelectric coupling term between mX_3^+, mX_1^- and Γ_4^-. We calculated the polarization after full ionic relaxation to be 4.88 μC cm^{-2}, which we believe to be one of the largest reported amongst spin-induced ferroelectrics, suggesting a strong trilinear coupling with this magnetic order. We compare this number with the purely electronic contribution to the polarization calculated with the ions fixed in the high-symmetry $Pm\bar{3}m$ positions, 0.07 μC cm^{-2}. This suggests the total polarization of 4.88 μC cm^{-2} is predominantly of ionic origin, which is also suggested by the reasonably large cation–anion off-centring in the ground-state structure (0.02 Å). Now that we have used these DFT calculations to illustrate our ideas, we will discuss the remaining magnetoelectric couplings based on symmetry arguments alone.

For $mX_5^+ \oplus mX_5^-$, the OP is now 12-dimensional OP(a,b;c,d;e,f|h,i;g,k;l,m). The representative (single k-active) OPDs which meet the criteria for zero crystal momentum transfer are however of the form OP(a,b;0,0;0,0|h,i;0,0;0,0). We do not consider OPs with multiple k-actives as in general this will always induce SOPs transforming as M- or R-point irreps,
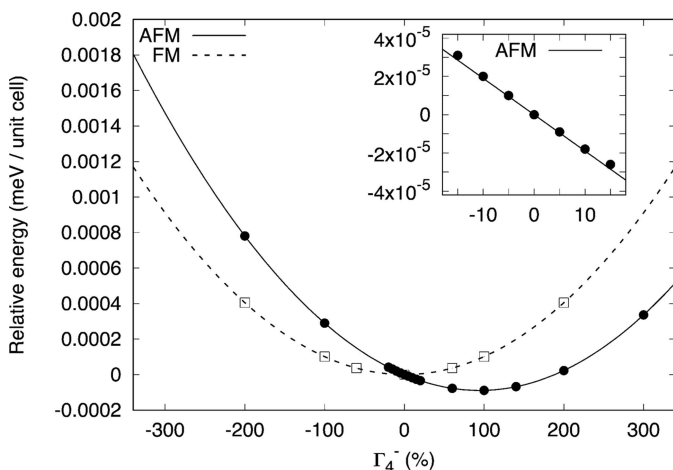
which are already covered in our previous analysis. We note here that we are not saying that these will correspond to physically equivalent examples, only that we can be sure that we have already considered the cases where linear terms in polarization will also be present in the free energy expansions. Hence the representative high-symmetry examples given in Fig. 4 are OP(a,a,0,0,0,0|h,$\bar{h}$,0,0,0,0) and OP(0,a,0,0,0,0|$\bar{h}$,0,0,0,0,0). We do not explicitly consider $mX_3^+ \oplus mX_5^-$ or $mX_5^+ \oplus mX_1^-$ here as these represent magnetic structures in which the spins on the A site and B site are noncollinear with each other, which we believe to be less physically likely than the remaining examples that we have already discussed.

For $mR_4^+ \oplus mR_5^-$, the resulting OP is OP(a,b,c|d,e,f). There are 14 possible OPDs that result in unique space-group, basis and origin combinations with respect to the parent structure. All other possible OPDs correspond to twin domains of these 14 possibilities. Of these 14 OPDs, we consider here three: OP(a,0,0|d,0,0), $I_c\bar{4}c2$, basis = [(-1, -1, 0),(1, -1, 0),(0, 0, 2)] + (0, 0, 0); OP(a,a,0|d,d,0), $I_c ma2$, basis = [(1, 0, 1),(1, 0, -1), (0, 2, 0)] + (0, $\frac{1}{2}$0, $-\frac{1}{2}$0); OP(a,a,a|d,d,d) R_I3c, basis = [(1, 0, -1),(0, -1, 1),(-2, -2, -2)] + (0, 0, 0), which correspond to collinear magnetic structures shown in Fig. 5. Any of the other lower-symmetry collinear magnetic structures may be constructed through linear combinations of these three OPDs. For the polar space groups ($I_c ma2$ and R_I3c) an SOP
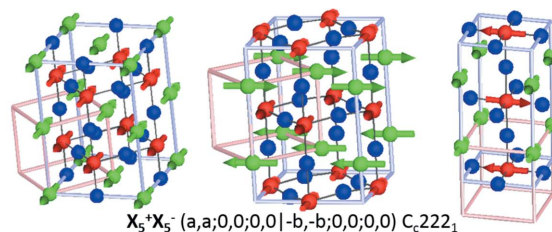

$X_5^+X_5^-$ (a,a;0,0;0,0| -b,-b;0,0;0,0) C_c222_1
$X_5^+X_5^-$(a,a;0,0;0,0|b,-b;0,0;0,0) $C_c mc2_1$ $X_5^+X_5^-$ (0,a;0,0;0,0|0,b;0,0;0,0) P_c222_1

Figure 4
Magnetic structures giving rise to the magnetoelectric effect resulting from the action of the OP(a,b,c|d,e,f) transforming as $mX_5^+ \oplus mX_5^-$, shown along the high-symmetry directions OP(a,a;0,0;0,0|d,$\bar{d}$;0,0;0,0), OP(a,a;0,0;0,0| $\bar{d}$,$\bar{d}$;0,0;0,0), OP(0,a;0,0;0,0|0,d,0,0;0,0).

POP: (mR_4^+|mR_5^-)

(a,0,0|d,0,0) I_c-4c2   (a,a,0|d,d,0) $I_c$ma2   (a,a,a|d,d,d)R_I3c
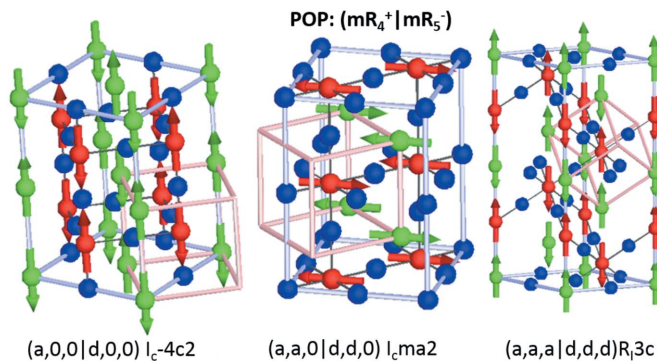
Figure 5
Collinear magnetic structures resulting from the action of the OP $(a, b, c \mid d, e, f)$ transforming as $mR_4^+ \oplus mR_5^-$, shown along the high-symmetry directions OP(a,0,0|d,0,0), OP(a,a,0|d,d,0), OP(a,a,a|d,d,d).

Figure 3
Energy *versus* polar mode [Γ_4^- OP(0,h,0)] magnitude for AFM [mX_3^+ mX_1^- OP(a,0,0|d,0,0)] and FM ($m\Gamma_4^+$) ordering. The inset illustrates the linear behaviour around the origin. The amplitude of the Γ_4^- mode is determined by summing the displacements of all the atoms in the unit cell and presented as a percentage with respect to the ground-state amplitude of the AFM phase. In both AFM and FM phases the energy shown is with respect to the structure with zero magnitude of Γ_4^-.

transforming as Γ_4^- is always active. The only other SOPs are strain. A strategy for stabilizing this ground-state structure, therefore, in addition to designing AFM nearest-neighbour interaction in the system, is to epitaxially pre-strain the sample in a manner that stabilizes terms in the free energy that will also occur at the even order.

$I_c\bar{4}c2$ (Fig. 5, left) on the other hand, although it has no inversion symmetry, is only piezoelectric. Indeed, it was very recently demonstrated (Zhao *et al.*, 2017) from a combination of first-principle calculations and group-theoretical analysis that the rare-earth gadolinium chromates and ferrites with collinear G-type order on *A* and *B* sites along the pseudo-cubic axes lead to a piezoelectric space group. Sheer strain along the [110]-type lattice directions was found to be needed to create a polarization through the piezoelectric effect, consistent with the piezoelectric point group. Our analysis shows an alternative route in which polarization emerges directly, provided that the spins align along the orthorhombic or rhombohedral type axes as in the cases discussed above of OP($a,a,0|d,d,0$) and OP($a,a,a|d,d,d$). We note also here that the possible observation of weak ferroelectric polarization, which is reported in *A*- and *B*-site lattices in which sub-lattice moments along 100-type directions are perpendicular to each other (Zhao *et al.*, 2017), may be understood in the framework of the SOP analysis that we have presented above. We find that Γ_4^- arises directly as a consequence of this kind of magnetic ordering [OP($a,0,0|0,0,d$)] with the magnetic space group being F_Smm2 {basis = [(0, 2, 0),(0, 0, 2),(2, 0, 0)], origin = $(\frac{1}{2}, \frac{1}{2}, 0)$}.

An experimental example of where magnetoelectric properties arise from G-type ordering on the *A* and *B* sites can be found in the literature for the 134 perovskite $LaMn_3Cr_4O_{12}$ (Wang *et al.*, 2015). This distorted perovskite structure has the additional structural orderings that can be described as $M_1^+(a;a;a)$ (1:3 cation ordering) and $M_2^+(a;a;a)$ (octahedral rotation). However, the observed magnetoelectric effect, that only occurs below both the *B*-site and the *A*-site ordering temperature, can be understood in terms of our present results by considering only OP $mR_4^+ \oplus mR_5^-$ with OP($a,a,a|d,d,d$) (Fig. 5, right), meaning that the magnetoelectric ground-state structure has rhombohedral lattice symmetry and arises solely as a consequence of the magnetic ordering on both sites.
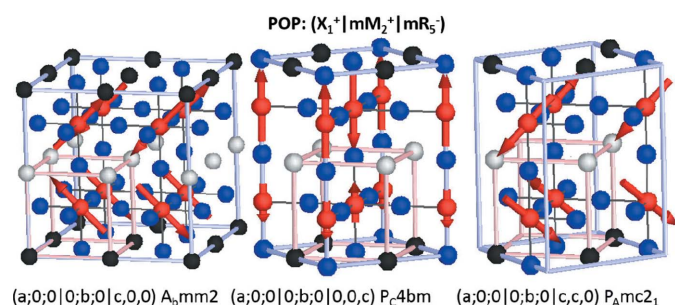
	mX_3^+ and mX_5^+	mX_1^- and mX_5^-
mM_2^+	R_2^-; R_3^-; R_4^-; R_5^-	R_1^+; R_5^+
mM_3^+	R_2^-; R_3^-; R_4^-; R_5^-	R_1^+; R_5^+
mM_5^+	R_2^-; R_3^-; R_4^-; R_5^-	R_1^+; R_5^+
	mX_3^+ and mX_5^+	mX_1^- and mX_5^-
mR_4^+	M_3^-; M_5^-	M_1^+; M_2^+; M_3^+; M_4^+
mR_5^-	M_1^+; M_2^+; M_3^+; M_4^+	M_3^-; M_5^-
	mM_2^+ and mM_3^+ and mM_5^+	
mR_4^+	X_3^-; X_5^-	
mR_5^-	X_1^+	

6. Fourth-order magnetoelectric couplings in AFM systems

An exhaustive list of fourth-order couplings in polarization and zone-boundary irreps is given in Table 2. There are naturally a large number of these, and we will restrict our more detailed discussion to those which are the most physically reasonable and likely to produce the strongest couplings at the highest ordering temperatures. Because of this, we will no longer consider magnetic ordering on the *A* site which in
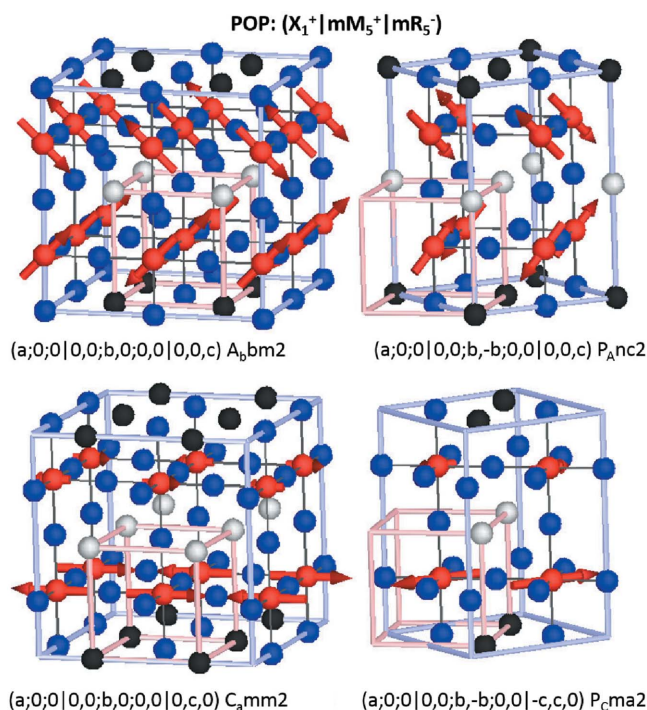
POP: ($X_1^+|mM_5^+|mR_5^-$)

(a;0;0|0,0;b,0;0,0|0,0,c) A_bbm2 (a;0;0|0,0;b,-b;0,0|0,0,c) P_Anc2

(a;0;0|0,0;b,0;0,0|0,c,0) C_amm2 (a;0;0|0,0;b,-b;0,0|-c,c,0) P_cma2

Figure 7
Magnetic structures giving rise to the magnetoelectric effect resulting from the action of the OP($a;b;c|d,e;f,g;h,i|j,k,l$) transforming as $X_1^+ \oplus mM_5^+ \oplus mR_5^-$, shown along the high-symmetry directions indicated. *A*-site cation ordering is indicated by white and black spheres.

POP: ($X_1^+|mM_2^+|mR_5^-$)

(a;0;0|0,b;0|c,0,0) A_bmm2 (a;0;0|0,b;0|0,0,c) P_c4bm (a;0;0|0,b;0|c,c,0) P_Amc2_1

Figure 6
Magnetic structures giving rise to the magnetoelectric effect resulting from the action of the OP($a;b;c|d;e;f|g, h, i$) transforming as $X_1^+ \oplus mM_2^+ \oplus mR_5^-$, shown along the high-symmetry directions indicated. *A*-site cation ordering is indicated by white and black spheres.

research papers

Table 3
Structural SOPs of POPs indicated in the table.

Polarization Γ_4^- is always an SOP.

POP	SOPs
$(X_1^+ \mid mM_2^+ \mid mR_5^-)$	
$(a;0\mid0\mid b;0\mid c,0,0)$	$\Gamma_3^+(a,b);\ \Gamma_4^-(0,0,a);\ \Gamma_5^-(a,0,0);\ X_2^+(a;0;0);\ X_5^-(a,0;0,0;0,0)$
$(a;0\mid0\mid b;0\mid0,0,c)$	$\Gamma_3^+(a,\sqrt{3}\bar{a});\ \Gamma_4^-(0,a,0);\ X_3^-(a;0;0)$
$(a;0\mid0\mid b;0\mid c,c,0)$	$\Gamma_3^+(a,\sqrt{3}\bar{a});\ \Gamma_5^+(0,0,a);\ \Gamma_4^-(a,0,a);\ \Gamma_5^-(a,\bar{a},0);\ X_5^-(a,a;0,0;0,0)$
$(X_1^+ \mid mM_5^+ \mid mR_5^-)$	
$(a;0\mid0\mid0,b;0,0,0\mid0,0,c)$	$\Gamma_3^+(a,b);\ \Gamma_4^-(a,0,0);\ \Gamma_5^-(0,a,0);\ X_2^+(a;0;0);\ X_5^-(0,a;0,0;0,0)$
$(a;0\mid0\mid0,b;0,0,0\mid0,c,0)$	$\Gamma_3^+(a,b);\ \Gamma_4^-(0,a,0);\ \Gamma_5^-(0,0,a);\ X_2^+(a;0;0);\ X_3^-(a;0;0)$
$(a;0\mid0\mid0,b;\bar{b},0,0\mid0,0,c)$	$\Gamma_3^+(a,\sqrt{3}\bar{a});\ \Gamma_5^+(0,0,a);\ \Gamma_4^-(a,0,\bar{a});\ \Gamma_5^-(a,a,0);\ X_5^-(a,\bar{a};0,0;0,0)$
$(a;0\mid0\mid0,b;\bar{b};0,0\mid \bar{c},c,0)$	$\Gamma_3^+(a,\sqrt{3}\bar{a});\ \Gamma_5^+(0,0,a);\ \Gamma_4^-(0,a,0);\ X_3^-(a;0;0)$

Table 4
Structural SOPs of POPs indicated in the table.

Polarization Γ_4^- is always an SOP.

POP	SOPs
$(mX_1^- \mid M_3^- \mid mR_5^-)$	
$(a;0\mid0\mid b;0\mid c,0,0)$	$\Gamma_3^+(a,b);\ \Gamma_4^-(a,0,0);\ \Gamma_5^-(0,a,0);\ M_5^+(0,0;a,0;0,0)$
$(a;0\mid0\mid b;0\mid c,c,0)$	$\Gamma_3^+(a,\sqrt{3}\bar{a});\ \Gamma_5^+(0,0,a);\ \Gamma_4^-(a,0,a);\ \Gamma_5^-(a,\bar{a},0);\ M_5^+(0,0;a,\bar{a};0,0);\ M_2^-(0;a;0)$
$(mX_5^- \mid M_3^- \mid mR_5^-)$	
$(a,\bar{a};0,0;0,0\mid0;b;0\mid0,0,c)$	$\Gamma_3^+(a,\sqrt{3}\bar{a});\ \Gamma_5^+(0,0,a);\ \Gamma_4^-(a,0,a);\ \Gamma_5^-(a,\bar{a},0);\ M_5^+(0,0;a,\bar{a};0,0);\ M_2^-(0;a;0)$
$(0,a;0,0;0,0\mid0;b;0\mid0,0,c)$	$\Gamma_3^+(a,b);\ \Gamma_4^-(a,0,0);\ \Gamma_5^-(0,a,0);\ M_5^+(0,0;a,0;0,0)$
$(0,a;0,0;0,0\mid0;b;0\mid0,c,0)$	$\Gamma_3^+(a,b);\ \Gamma_4^-(0,a,0);\ \Gamma_5^-(0,0,a);\ M_1^+(0;a;0);\ M_2^+(0;a;0)$
$(a,\bar{a};0,0;0,0\mid0;b;0\mid c,c,0)$	$\Gamma_3^+(a,\sqrt{3}\bar{a});\ \Gamma_5^+(0,0,a);\ \Gamma_4^-(0,a,0);\ M_1^+(0;a;0);\ M_4^+(0;a;0);\ M_2^-(0;a;0)$
$(mX_1^- \mid M_5^- \mid mR_5^-)$	
$(a;0\mid0,0;b;0,0\mid c,0,0)$	$\Gamma_3^+(a,b);\ \Gamma_4^-(0,a,0);\ \Gamma_5^-(0,0,a);\ M_5^+(0,0;a,0;0,0)$
$(a;0\mid0,0;0,0;b;0,0\mid0,0,c)$	$\Gamma_3^+(a,b);\ \Gamma_4^-(0,0,a);\ \Gamma_5^-(a,0,0);\ M_3^+(0;a;0);\ M_4^+(0;a;0)$
$(a;0\mid0,0;b,b;0,0\mid0,0,c)$	$\Gamma_3^+(a,\sqrt{3}\bar{a});\ \Gamma_5^+(0,0,a);\ \Gamma_4^-(a,0,a);\ \Gamma_5^-(a,\bar{a},0);\ M_1^+(0;a;0);\ M_4^+(0;a;0)$
$(a;0\mid0,0;b,b;0,0\mid c,c,0)$	$\Gamma_3^+(a,\sqrt{3}\bar{a});\ \Gamma_5^+(0,0,a);\ \Gamma_4^-(0,a,0);\ M_5^+(0,0;a,\bar{a};0,0)$
$(mX_5^- \mid M_5^- \mid mR_5^-)$	
$(0,a;0,0;0,0\mid0,0;0,b;0,0\mid c,0,0)$	$\Gamma_3^+(a,b);\ \Gamma_4^-(0,0,a);\ \Gamma_5^-(a,0,0);\ M_3^+(0;a;0);\ M_4^+(0;a;0)$
$(0,a;0,0;0,0\mid0,0;0,b;0,0\mid0,0,c)$	$\Gamma_3^+(a,b);\ \Gamma_4^-(0,a,0);\ \Gamma_5^-(0,0,a);\ M_5^+(0,0;a,0;0,0)$
$(0,a;0,0;0,0\mid0,0;0,b;0,0\mid0,c,0)$	$\Gamma_3^+(a,b);\ \Gamma_4^-(a,0,0);\ \Gamma_5^-(0,a,0);\ M_1^+(0;a;0);\ M_2^+(0;a;0)$
$(0,a;0,0;0,0\mid0,0;\bar{b},0;0,0\mid0,c,0)$	$\Gamma_3^+(a,b);\ \Gamma_4^-(a,0,0);\ \Gamma_5^-(0,a,0);\ M_3^+(0;a;0);\ M_4^+(0;a;0)$
$(0,a;0,0;0,0\mid0,0;\bar{b},0;0,0\mid0,c,0)$	$\Gamma_3^+(a,b);\ \Gamma_4^-(0,0,a);\ \Gamma_5^-(a,0,0);\ M_1^+(0;a;0);\ M_2^+(0;a;0)$
$(a,\bar{a};0,0;0,0\mid0,0;b,b;0,0\mid0,0,c)$	$\Gamma_3^+(a,\sqrt{3}\bar{a});\ \Gamma_5^+(0,0,a);\ \Gamma_4^-(0,a,0);\ M_5^+(0,0;a,\bar{a};0,0)$
$(a,\bar{a};0,0;0,0\mid0,0;b,b;0,0\mid c,c,0)$	$\Gamma_3^+(a,\sqrt{3}\bar{a});\ \Gamma_5^+(0,0,a);\ \Gamma_4^-(a,0,a);\ \Gamma_5^-(a,\bar{a},0);\ M_1^+(0;a;0);\ M_4^+(0;a;0)$
$(a,\bar{a};0,0;0,0\mid0,0;b,b;0,0\mid \bar{c},c,0)$	$\Gamma_3^+(a,\sqrt{3}\bar{a});\ \Gamma_5^+(0,0,a);\ \Gamma_4^-(a,0,\bar{a});\ \Gamma_5^-(a,a,0);\ M_2^-(0;a;0);\ M_3^-(0;a;0)$
$(a,\bar{a};0,0;0,0\mid0,0;\bar{b},b;0,0\mid c,c,0)$	$\Gamma_3^+(a,\sqrt{3}\bar{a});\ \Gamma_5^+(0,0,a);\ \Gamma_4^-(a,0,\bar{a});\ \Gamma_5^-(a,a,0);\ M_1^+(0;a;0);\ M_4^+(0;a;0)$
$(a,\bar{a};0,0;0,0\mid0,0;\bar{b},b;0,0\mid \bar{c},c,0)$	$\Gamma_3^+(a,\sqrt{3}\bar{a});\ \Gamma_5^+(0,0,a);\ \Gamma_4^-(a,0,a);\ \Gamma_5^-(a,\bar{a},0);\ M_2^-(0;a;0);\ M_3^-(0;a;0)$

general only supports rare-earth ions or non-magnetic cations. Notable exceptions to this are the perovskite MnVO$_3$, but where the magnetic ordering temperatures remain low (Markkula *et al.*, 2011), and some highly distorted $AA'_3B_4O_{12}$ quadruple perovskites that we will not discuss here.

Considering only *B*-site magnetism we are left with the following time-odd superposition of irreps to consider: $mM_{2,5}^+ \oplus mX_{1,5}^-$; $mR_5^- \oplus mX_{1,5}^-$; $mR_5^- \oplus mM_{2,5}^+$. In order to close the 'momentum triangle' these will now be, respectively, superposed with the following time-even irreps: $R_{1,5}^+$, $M_{3,5}^-$ and X_1^+, to produce an OP that transforms as time-even, inversion-odd and has a crystal momentum transfer of zero (see Tables 3, 4 and 5). The relevant structural degrees of freedom (Table 1) to consider are, hence, cation/anion order (X_1^+, $R_{1,5}^+$) and antipolar displacements ($M_{3,5}^-$). Notably, octahedral tilts or Jahn–Teller modes do not appear in this list and hence cannot form part of such a design strategy.

For $X_1^+ \oplus mM_{2,5}^+ \oplus mR_5^-$ we give some possible examples of several magnetic structures in Figs. 6 and 7 corresponding to *A*-site ordered double perovskites with striped type (X_1^+) arrangements of cations, such as is commonly found experimentally for cations of substantially different sizes (King & Woodward, 2010). Some of these compounds are already known to be improper ferroelectric (Zuo *et al.*, 2017) on account of couplings between the layering and octahedral tilt modes, as discussed in the previous section.

The possible high-symmetry OPDs for superposed irreps $X_1^+(0, \frac{1}{2}, 0) \oplus mM_2^+(\frac{1}{2}, \frac{1}{2}, 0) \oplus mR_5^-(\frac{1}{2}, \frac{1}{2}, \frac{1}{2})$ are:

$(a;0\mid0\mid0;b;0\mid c,0,0);\ (a;0\mid0\mid0;b;0\mid0, 0, c);\ (a;0\mid0\mid0;b;0\mid c,c,0).$

Conservation of crystal momentum criteria that we have imposed here dictates the relative OPD of the X and M components (*k*-actives). The three structures listed above and shown in Fig. 6 only differ in the OPD with respect to the mR_5^- irrep, producing two non-collinear magnetic structures and one which has a spin-density-wave. In the case of the non-collinear magnetic structures, the direction of P is parallel to both the cation order planes and the magnetic moment canting

Table 5
Structural SOPs of POPs indicated in the table.

Polarization Γ_4^- is always an SOP.

POP	SOPs
$(mX_1^- \mid mM_2^+ \mid R_5^+)$	
$(a;0\mid0;b;0\mid c,0,0)$	$\Gamma_3^+(a,b)$; $\Gamma_4^-(0,0,a)$; $\Gamma_5^-(a,0,0)$; $R_2^-(a)$; $R_3^-(a,b)$
$(a;0\mid0;b;0\mid0,0,c)$	$\Gamma_3^+(a,\sqrt{3}\bar{a})$; $\Gamma_4^-(0,a,0)$; $R_2^-(a)$; $R_3^-(a,\sqrt{3}\bar{a})$
$(a;0\mid0;b;0\mid c,c,0)$	$\Gamma_3^+(a,\sqrt{3}\bar{a})$; $\Gamma_5^+(0,0,a)$; $\Gamma_4^-(a,0,a)$; $\Gamma_5^-(a,\bar{a},0)$; $R_2^-(a)$; $R_3^-(a,\sqrt{3}\bar{a})$; $R_4^-(0,0,a)$
$(mX_1^- \mid mM_5^+ \mid R_5^+)$	
$(a;0\mid0,0;b,0;0,0\mid0,0,c)$	$\Gamma_3^+(a,b)$; $\Gamma_4^-(a,0,0)$; $\Gamma_5^-(0,a,0)$; $R_4^-(a,0,0)$; $R_5^-(a,0,0)$
$(a;0\mid0,0;b,0;0,0\mid0,c,0)$	$\Gamma_3^+(a,b)$; $\Gamma_4^-(0,a,0)$; $\Gamma_5^-(0,0,a)$; $R_4^-(a,0,0)$; $R_5^-(a,0,0)$
$(a;0\mid0,0;b,\bar{b};0,0\mid0,0,c)$	$\Gamma_3^+(a,\sqrt{3}\bar{a})$; $\Gamma_5^+(0,0,a)$; $\Gamma_4^-(a,0,\bar{a})$; $\Gamma_5^-(a,a,0)$; $R_4^-(a,\bar{a},0)$; $R_5^-(a,a,0)$
$(a;0\mid0,0;b,\bar{b};0,0\mid\bar{c},c,0)$	$\Gamma_3^+(a,\sqrt{3}\bar{a})$; $\Gamma_5^+(0,0,a)$; $\Gamma_4^-(0,a,0)$; $R_4^-(a,\bar{a},0)$; $R_5^-(a,a,0)$
$(mX_5^- \mid mM_2^+ \mid R_5^+)$	
$(a,\bar{a};0,0\mid0,0\mid0;b;0\mid0,0,c)$	$\Gamma_3^+(a,\sqrt{3}\bar{a})$; $\Gamma_5^+(0,0,a)$; $\Gamma_4^-(a,0,a)$; $\Gamma_5^-(a,\bar{a},0)$; $R_4^-(a,a,0)$; $R_5^-(a,\bar{a},0)$
$(0,a;0,0\mid0,0\mid0;b;0\mid c,0,0)$	$\Gamma_3^+(a,b)$; $\Gamma_4^-(0,a,0)$; $\Gamma_5^-(0,0,a)$; $R_4^-(0,a,0)$; $R_5^-(0,a,0)$
$(0,a;0,0\mid0,0\mid0;b;0\mid0,0,c)$	$\Gamma_3^+(a,b)$; $\Gamma_4^-(0,a,0)$; $\Gamma_5^-(a,0,0)$; $R_4^-(0,a,0)$; $R_5^-(0,a,0)$
$(a,\bar{a};0,0\mid0,0\mid0;b;0\mid c,c,0)$	$\Gamma_3^+(a,\sqrt{3}\bar{a})$; $\Gamma_5^+(0,0,a)$; $\Gamma_4^-(0,a,0)$; $R_4^-(a,a,0)$; $R_5^-(a,\bar{a},0)$
$(mX_5^- \mid mM_5^+ \mid R_5^+)$	
$(0,a;0,0,0\mid0,0;b,0;0,0\mid c,0,0)$	$\Gamma_3^+(a,b)$; $\Gamma_4^-(a,0,0)$; $\Gamma_5^-(0,a,0)$; $R_4^-(0,0,a)$; $R_5^-(0,0,a)$
$(0,a;0,0,0\mid0,0;b,0;0,0\mid0,c,0)$	$\Gamma_3^+(a,b)$; $\Gamma_4^-(0,a,0)$; $\Gamma_5^-(0,0,a)$; $R_4^-(0,0,a)$; $R_5^-(0,0,a)$
$(0,a;0,0,0\mid0,0;b,\bar{b};0,0\mid c,0,0)$	$\Gamma_3^+(a,b)$; $\Gamma_4^-(0,0,a)$; $\Gamma_5^-(a,0,0)$; $R_2^-(a)$; $R_3^-(a,b)$
$(0,a;0,0,0\mid0,0;b,\bar{b};0,0\mid0,0,c)$	$\Gamma_3^+(a,b)$; $\Gamma_4^-(0,a,0)$; $\Gamma_5^-(0,0,a)$; $R_2^-(a)$; $R_3^-(a,b)$
$(0,a;0,0,0\mid0,0;b,\bar{b};0,0\mid0,c,0)$	$\Gamma_3^+(a,b)$; $\Gamma_4^-(a,0,0)$; $\Gamma_5^-(0,a,0)$; $R_2^-(a)$; $R_3^-(a,b)$
$(a,\bar{a};0,0,0\mid0,0;b,\bar{b};0,0\mid0,0,c)$	$\Gamma_3^+(a,\sqrt{3}\bar{a})$; $\Gamma_5^+(0,0,a)$; $\Gamma_4^-(0,a,0)$; $R_2^-(a)$; $R_3^-(a,\sqrt{3}\bar{a})$; $R_4^-(0,0,a)$
$(a,\bar{a};0,0,0\mid0,0;b,\bar{b};0,0\mid c,c,0)$	$\Gamma_3^+(a,\sqrt{3}\bar{a})$; $\Gamma_5^+(0,0,a)$; $\Gamma_4^-(a,0,\bar{a})$; $\Gamma_5^-(a,a,0)$; $R_3^-(a,0.577a)$; $R_5^-(0,0,a)$
$(a,\bar{a};0,0,0\mid0,0;b,\bar{b};0,0\mid\bar{c},c,0)$	$\Gamma_3^+(a,\sqrt{3}\bar{a})$; $\Gamma_5^+(0,0,a)$; $\Gamma_4^-(a,0,a)$; $\Gamma_5^-(a,\bar{a},0)$; $R_3^-(a,0.577a)$; $R_5^-(0,0,a)$
$(a,\bar{a};0,0,0\mid0,0;b,\bar{b};0,0\mid c,c,0)$	$\Gamma_3^+(a,\sqrt{3}\bar{a})$; $\Gamma_5^+(0,0,a)$; $\Gamma_4^-(a,0,a)$; $\Gamma_5^-(a,\bar{a},0)$; $R_2^-(a)$; $R_3^-(a,\sqrt{3}\bar{a})$; $R_4^-(0,0,a)$
$(a,\bar{a};0,0,0\mid0,0;b,\bar{b};0,0\mid\bar{c},c,0)$	$\Gamma_3^+(a,\sqrt{3}\bar{a})$; $\Gamma_5^+(0,0,a)$; $\Gamma_4^-(a,0,\bar{a})$; $\Gamma_5^-(a,a,0)$; $R_2^-(a)$; $R_3^-(a,\sqrt{3}\bar{a})$; $R_4^-(0,0,a)$

direction. For the spin-density-wave structure the polarization vector is perpendicular to the cation ordering planes. Spin-density-wave magnetic structures are in general less common, but we note that X-point order of two magnetically active cations (at the B site) with different magnetic moments could be a way to achieve this.

For $X_1^+ \oplus mM_5^+ \oplus mR_5^-$ as mM_5^+ is a higher-dimensional irrep than M_2^+, there are now a larger number of OPD possibilities:

$(a;0;0\mid0,0;b,0;0,0\mid c,0,0)$; $(a;0;0\mid0,0;b,0;0,0\mid0,0,c)$;

$(a;0;0\mid0,0;b,0;0,0\mid0,c,0)$; $(a;0;0\mid0,0;b,-b;0,0\mid0,0,c)$;

$(a;0;0\mid0,0;b,-b;0,0\mid c,c,0)$; $(a;0;0\mid0,0;b,-b;0,0\mid-c,c,0)$.

However, this time several of these high-symmetry OPs give rise to piezoelectric but non-polar space groups [$(a;0;0\mid0,0;b,0;0,0\mid c,0,0)$ $C222$ and $(a;0\mid0,0;b,-b;0,0\mid c,c,0)$ $P222_1$]. Although not ferroelectric, the inclusion of any further POP either as an internal or external strain field will drive a ferroelectric ground state in these systems. Fig. 7 shows the representative high-symmetry OPD resulting in polar structures. Similarly for the discussion above, P is parallel and perpendicular to cation ordering for constant moment and spin-density-wave magnetic structures, respectively.

For $mX_{1,5}^- \oplus mM_{2,5}^+ \oplus R_5^+$, in which R_5^+ could correspond to anion order, the *cis*-ordering of N for O substitution in oxynitride $ABO_{3-x}N_x$ perovskite (Yang *et al.*, 2011) represents an experimental realization of this. For $x = 1.5$, this would correspond to a checkerboard anion order and hence we consider $R_5^+(a,a,a)$ (or the closest high-symmetry equivalent OPD) in the following analysis. As a POP transforming as $R_5^+(a,a,a)$ always has an SOP transforming as $R_1^+(a)$, this analysis also turns out to be equivalent to looking at rocksalt

ordering on the A-site cation, although we note that such ordering is not particularly common. $mX_1^-(0,\frac{1}{2},0)$ $mM_2^+(\frac{1}{2},\frac{1}{2},0)$ $R_5^+(\frac{1}{2},\frac{1}{2},\frac{1}{2})$, with an OPD of $(a;0\mid0;b;0\mid c,c,d)$, corresponds to a spin-density-wave collinear magnetic structure, where P is in

POP: $(mX_1^- \mid mM_2^+ \mid R_5^+)$

$(a;0;0\mid0;b;0\mid c,c,d)$ P_Ac

POP: $(mX_5^- \mid mM_2^+ \mid R_5^+)$

$(a,-a;0,0;0,0\mid0;b;0\mid c,c,d)$ P_Ac $(a,-a;0,0;0,0\mid0;b;0\mid-c,c,-d)P_C2_1$
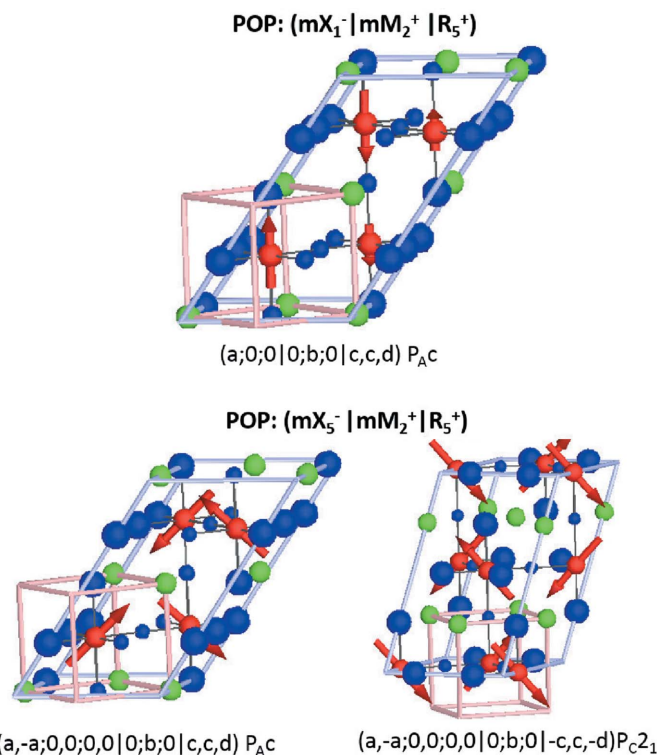
Figure 8
Magnetic structures giving rise to the magnetoelectric effect resulting from the action of the OP as shown along the high-symmetry directions indicated. Anion ordering is indicated by blue spheres of differing sizes.
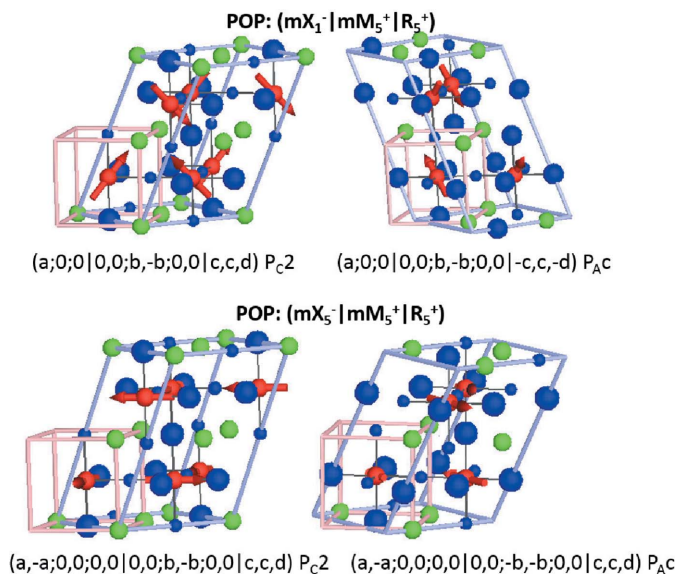
POP: $(mX_1^-|mM_5^+|R_5^+)$

$(a;0;0|0,0;b,-b;0,0|c,c,d)$ P_C2 $(a;0;0|0,0;b,-b;0,0|-c,c,-d)$ P_AC

POP: $(mX_5^-|mM_5^+|R_5^+)$

$(a,-a;0,0;0,0|0,0;b,-b;0,0|c,c,d)$ P_C2 $(a,-a;0,0;0,0|0,0;-b,-b;0,0|c,c,d)$ P_AC

Figure 9
Magnetic structures giving rise to the magnetoelectric effect resulting from the action of the OP as shown along the high-symmetry directions indicated. Anion ordering is indicated by blue spheres of differing sizes.

$(mX_1^-|M_3^-|mR_5^-)$ $(mX_1^-|M_5^-|mR_5^-)$

$(a;0;0|0;b;0|c,0,0)$ A_aba2 $(a;0;0|0,0;0,b;0,0|c,0,0)$ C_ccc2

$(mX_5^-|M_3^-|mR_5^-)$ $(mX_5^-|M_5^-|mR_5^-)$

$(0,a;0,0;0,0|0;b;0|0,0,c)$ A_abm2 $(0,a;0,0;0,0|0,0;0,b;0,0|c,0,0)$ A_ama2

Figure 10
Magnetic structures giving rise to the magnetoelectric effect resulting from the action of the OP as shown along the high-symmetry directions indicated.

the plane of the magnetic moment directions (Fig. 8). The constant-magnitude spin-canted magnetic structures $[mX_5^- \oplus mM_2^+ \oplus R_5^+$ $(a;0;0|b;0|c,c,d)$, Fig. 8] on the other hand lead to polarizations that are found to be both perpendicular and parallel to the magnetic moment alignment.

We will not consider the remaining possible couplings for $mX_1^- \oplus mM_2^+ \oplus R_5^+$, $mX^- \oplus mM_5^+ \oplus R_5^+$ and $mX_1^- \oplus M^- \oplus mR_5^-$ explicitly here but they are tabulated in Table 5 and representative figures are given in Figs. 8, 9 and 10.

7. Stabilizing wFM and magnetoelectric effects in non-ferroelectrics

For multiferroics to be useful in data storage applications, it is likely that they will need to have a ferromagnetically ordered and switchable component. Following the design strategy above we wish to engineer a trilinear term in the free energy expansion of the form A B wFM. Since wFM transforms as $m\Gamma_4^+$ which is time-odd, parity-even and has crystal momentum of zero, the constraints on A and B are as follows:

[A] = [B]

A·B is parity-even.

Hence, possible trilinear terms with wFM need to involve OPs that transform as:

$$mR^- \oplus R^-; \ mR^+ \oplus R^+; \ mM^+ \oplus M^+; \ mX^- \oplus X^-; \ mX^+ \oplus X^+.$$

Taking mR_5^- (B-site magnetic order) with R_5^- (octahedral tilting) as an example, G-type magnetic ordering on the B sites with moments along the c axis with out-of-phase octahedral rotations leads to the magnetic space group $Im'm'a$ {basis = $[(1, 1, 0),(0, 0, 2),(1, -1, 0)] + (0, 0, \frac{1}{2})$} which has $m\Gamma_4^+$ (wFM) as an SOP. Indeed, we believe this is the framework by which the theoretically predicted wFM in Gd Cr/Fe perovskites
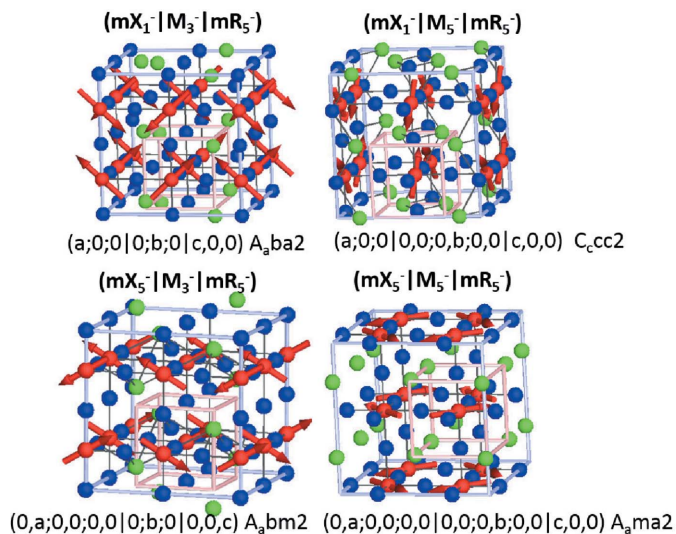
(Zhao *et al.*, 2017; Tokunaga *et al.*, 2009) can be easily understood, and is an example in which the B—O—B exchange angle is allowed to deviate from 180° by a symmetry-breaking event allowing spin canting to occur *via* the Dzyaloshinsky–Moriya interaction.

At the M-point the above analysis can also be applied. C-type B-site magnetic ordering along the [001] axis $[mM_2^+(a;0;0)]$, with in-phase octahedral tilts perpendicular to this $[M_2^+(a;0;0), a^0a^0c^+]$, actually leads to a piezomagnetic space group $P4/mbm$ {basis = $[(1, -1, 0),(1, 1, 0),(0, 0, 1)] + (\frac{1}{2}, -\frac{1}{2}, 0)$}. Application of an orthorhombic type strain (Γ_5^+) for example leads to the occurrence of wFM ($m\Gamma_4^+$). Similarly, distortions transforming as X_5^- and magnetic moments as mX_1^- will produce wFM {*e.g.* $Cm'cm'$, basis = $[(1, 0, 1), (1, 0, -1),(0, 2, 0)] + (0, \frac{1}{2}, 0)$}.

Another magnetoelectric effect worth considering is where P is induced by the application of an external magnetic field which may be described as transforming as $m\Gamma_4^+$ or conversely wFM is induced by the application of an external electric field (Γ_4^-). For this we must look at terms involving two zone-boundary irreps like [M] + [S] = [0 0 0], where M is time-odd (magnetic) and S is time-even (structural), and M·S is inversion-odd. Application of an electric field (Γ_4^-) should then give a fourth-order term in the free energy expansion of the form M S P wFM. A realization of this is $mX_{1,5}^- \oplus X_1^+ \oplus P$, to give wFM. Finally it is worth pointing out that all systems that are both piezoelectric and piezomagnetic will be magnetoelectric, as application of either an external magnetic or electric field will generate a strain field that mediates a coupling between the two phenomena.

8. Putting it all together

The ultimate goal of course is to have a magnetoelectric in which ferromagnetism is coupled to ferroelectricity. To

achieve the strongest such coupling, we envisage first a scenario with two trilinear terms in P and wFM, with one co-dependent OP (see Fig. 11). For example: (i) $X_1^+ \oplus X_5^- \oplus P$ with $mX_1^- \oplus X_5^- \oplus$ wFM. Assuming X_1^+ represents cation order and may not be reversed, then the reversal of the sign of P would necessitate a reversal of X_5^-. This, in turn, would necessitate a switching of the magnetic structure which most likely would proceed *via* a reversal of the direction of the wFM. (ii) $M_5^- \oplus M_2^+ \oplus P$ and $mM_5^- \oplus M_2^+ \oplus$ wFM. Taking M_5^- as anion ordering, then a reversal of P would proceed *via* reversal of the octahedral rotations (M_2^+) necessitating a reversal of either mM_5^- or wFM, the latter being more likely. (iii) $R_1^+ \oplus R_2^- \oplus P$ and $mR_5^- \oplus R_2^- \oplus$ wFM, taking R_1^+ as *A*-site rocksalt cation ordering, a reversal of P would imply a switching of R_2^- which could represent *B*-site charge ordering

In fact, if one has an AA' layered double perovskite (X_1^+) with the common M_2^+ and R_5^- tilt pattern (*Pnma* like) no matter if you have C (mM_5^+), G (mR_5^-) or A (mX_1^-) magnetic ordering (provided the spins are along certain directions), the ground state is ferroelectric and ferromagnetic with an indirect coupling between them. Efforts should hence be focused on preparing $A^+ A'^{3+}$ and $A^{2+} A'^{4+}$ layered double perovskites with Mn^{4+} and Fe^{3+} on the *B* site, respectively, to achieve the strongest wFM moments and highest ordering temperatures.

Another scheme involving fourth-order couplings gives a greater degree of flexibility. Similar to the above, the idea here is to construct fourth-order terms with wFM ($m\Gamma_4^+$) in. As many of the OPs featuring in the wFM term at the fourth order should also feature in the fourth-order term in P. Fig. 12 envisages one such possible coupling scheme by which an extra degree of freedom related to breaking structural symmetry (S_2) is introduced to the magnetoelectric couplings discussed above, and is equivalent to using antisymmetric (DM) arguments to design wFM. The figure shows that it is possible to construct fourth-order terms with at least two OPs in common in both P and wFM terms, *i.e.* $M_1 M_2 S_1 P$ and $M_1 S_1 S_2$ wFM. Each fourth-order term must individually conserve crystal momentum, time reversal and inversion symmetry. Hence the polar part, $M_1 M_2 S_1$, can be selected according to the analysis in the previous section, leaving the wFM part, $M_1 S_1 S_2$, to be decided on. Since $M_1 S_1$ are fixed by the polar part, the only decision to be made is the nature of S_2. We require that the crystal momentum of $[S_2]$ equals the sum of the crystal momentum $[M_1] + [S_1]$, and that parity with respect to inversion is equal to the product of the parity of $M_1 \cdot S_1$ (*i.e.* opposite to that of M_2). For example, with $mM_{2,5}^+$ (M), mR_5^- (M) and X_1^+ (S_1), S_2 must be either $R_{1,5}^+$ or $M_{2,3,5}^+$.
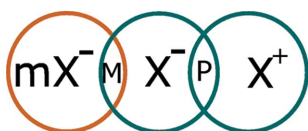

Figure 11
A scheme for including third-order coupling terms in the free energy expansion involving the OP related to weak ferromagnetic spin canting and ferroelectric polarization.
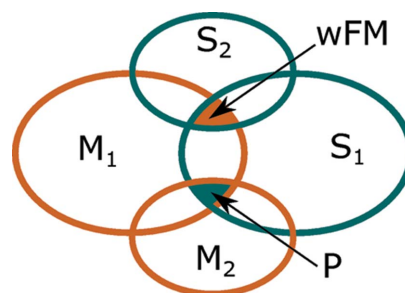

Figure 12
A scheme for including fourth-order coupling terms in the free energy expansion involving the OP related to weak ferromagnetic spin canting and ferroelectric polarization.

Finally, we note that if one predisposes the system to certain distortions, which are implied as SOPs in the above analysis, certain phases may be thermodynamically favoured over others. This is an important part of controlling the relative OPDs which ultimately affect the higher-order couplings that drive magnetoelectric properties. We discuss now a few of the most promising candidates and propose some design strategies based on SOP analysis. SOPs are listed in Tables 3, 4 and 5 for some fourth-order couplings in ferroelectric polarization. Any further distortion to the $Pm\bar{3}m$ aristotype that the system is predisposed to, which transforms as irreps in this list, will act to stabilize one particular OPD over another. Or, put another way, at the harmonic order (quadratic phonon modes) all possible OPDs are degenerate in energy.

The most obvious strategy is to pre-strain (transforming as $\Gamma_{3,5}^+$) the system through epitaxial growth. Another strategy is to search through tables, such as Tables 3, 4 and 5, to find irreps that correspond to the most commonly observed distortions in the perovskite phase, such as the octahedral rotations (M_2^+ and R_5^-), Jahn–Teller distortions in systems with a degeneracy in their *d* orbitals or indeed polar distortions themselves in d^0 systems. In the 'undistorted' perovskite structure these will correspond to the lowest-lying phonon modes (rigid unit modes in the cases of the octahedral rotation). Any energy penalty paid at the quadratic order will be kept low with respect to the trilinear terms that always act to lower the free energy, and therefore will drive a phase transition. For example, for $X_1^+ \oplus mM_2^+ \oplus mR_5^-$, SOPs are strain, Γ_5^-, and X-point distortions. The OP(a;0;0|0;b;0|c,c,0) P_Amc2_1 is the most promising candidate, as the only SOP is antipolar X5− distortions. Therefore, in addition to striped cation ordering, cations which are susceptible to off-centre distortions should be chosen. For $mX_1^- \oplus M_5^- \oplus mR_5^-$ or $mX_1^- \oplus mM_2^+ \oplus R_5^+$, *B* sites with a propensity to undergo charge (M_4^+ or R_2^-) and orbital order (M_3^+ or R_3^-) should be chosen. A similar design strategy of selecting a system which is predisposed to certain SOPs may be adopted for stabilizing wFM.

9. Conclusion

Using group-theoretical means, we have enumerated the possible magnetoelectric couplings in the perovskite structure with respect to its aristotypical symmetry $Pm\bar{3}m$. Our

enumeration is complete up to the third-order terms for zone-boundary magnetic structures, and for fourth-order terms for B-site magnetism only. Our results show that, for zone-boundary magnetic ordering, only magnetism on both A and B sites transforming either both as X-point or R-point irreps can produce a magnetoelectric coupling at the third order, which is illustrated with first-principles calculations. For magnetism on the B site alone, then only fourth-order terms can produce the desired effect. We propose a design strategy based on POPs consisting of a superposition of three irreps, one each from the X-, M- and R-points, chosen in such a way that crystal momentum is conserved, that two are time-odd and either one or all are inversion-odd. These ideas are extended to a design strategy for weak ferromagnetism, which may then be coupled to the ferroelectric polarization in a similar manner to the recently much discussed hybrid improper ferroelectric $Ca_3Mn_2O_7$. Without a doubt, predicting and controlling physical properties arising from magnetic order will remain a challenging area for many years to come. However, our systematic enumeration of coupling mechanisms along with secondary order parameters at least provides some direction for how this might ultimately be achieved.

APPENDIX A
Notation used in order parameter directions

We will be forming OPs from up to three different zone-boundary irreps, which we will denote by using the symbol for direct sum '$\oplus$', for example $M_2^+ \oplus R_5^-$ represents an OP that has atomic displacements that transform as both irreps. By forming this OP we will effectively be conducting a thought experiment as to what would happen if the parent $Pm\bar{3}m$ became spontaneously unstable with respect to atomic displacements (in this case octahedral rotations) transforming as these irreps. However, specifying these irreps alone does not capture how the displacements (or magnetic orderings) combine with respect to each other, and hence the associated isotropy subgroup. To do this we need to describe the full OPD of the OP transforming as the specified irreps and we follow the notation used in *ISODISRORT* (Campbell *et al.*, 2006). For $M_2^+ \oplus R_5^-$, an OPD is OP(a;0;0|b,0,0), where '|' denotes a division between the OPD parts belonging to M_2^+ and R_5^-, respectively. Semi-colons ';' denote divisions between different OPDs resulting from the degeneracy of the propagation vector in $Pm\bar{3}m$. At the M-point the possible k-actives are $(\frac{1}{2}, \frac{1}{2}, 0)$;$(\frac{1}{2}, 0, \frac{1}{2})$;$(0, \frac{1}{2}, \frac{1}{2})$, where the order respects the order of appearance in the OPD. Similarly, for an OP transforming as X-point irreps we will need to specify which k-actives of $(0, \frac{1}{2}, 0)$;$(\frac{1}{2}, 0, 0)$;$(0, 0, \frac{1}{2})$ are in use. In general we will only form OPs from one k-active per irrep (equivalent to using the small irrep only). However, the notation we give will always reflect the total number of possible k-actives. At the R-point there is only one possible k-active, but in this case the irrep is multidimensional and, as in the case of Γ_4^-, this is specified through use of commas between the letters. The total dimension of the OP is hence a function of the number of superposed irreps, the

degeneracy of the propagation vectors associated with any of the irreps and the dimensionality of the small irreps themselves. All need to be fully specified along with the setting and space group of the parent structure to uniquely identify the isotropy subgroup.

References

Aimi, A., Mori, D., Hiraki, K., Takahashi, T., Shan, Y. J., Shirako, Y., Zhou, J. & Inaguma, Y. (2014). *Chem. Mater.* **26**, 2601–2608.
Aleksandrov, K. S. & Bartolome, J. (1994). *J. Phys. Condens. Matter*, **6**, 8219–8235.
Aroyo, M. I., Kirov, A., Capillas, C., Perez-Mato, J. M. & Wondratschek, H. (2006). *Acta Cryst.* A**62**, 115–128.
Benedek, N. A. & Fennie, C. J. (2011). *Phys. Rev. Lett.* **106**, 107204.
Benedek, N. A., Rondinelli, J. M., Djani, H., Ghosez, P. & Lightfoot, P. (2015). *Dalton Trans.* **44**, 10543–10558.
Boström, H. L. B., Senn, M. S. & Goodwin, A. L. (2018). *Nat. Commun.* **9**, 2380.
Bousquet, E., Dawber, M., Stucki, N., Lichtensteiger, C., Hermet, P., Gariglio, S., Triscone, J.-M. & Ghosez, P. (2008). *Nature*, **452**, 732–736.
Bradley, C. J. C. J. & Cracknell, A. P. (1972). *The Mathematical Theory of Symmetry in Solids: Representation Theory for Point Groups and Space Groups*. Oxford: Clarendon Press.
Bristowe, N. C., Varignon, J., Fontaine, D., Bousquet, E. & Ghosez, P. (2015). *Nat. Commun.* **6**, 6677.
Campbell, B. J., Evans, J. S. O., Perselli, F. & Stokes, H. T. (2007). *IUCr Comput. Commun. Newsl.* **8**, 81–95.
Campbell, B. J., Stokes, H. T., Tanner, D. E. & Hatch, D. M. (2006). *J. Appl. Cryst.* **39**, 607–614.
Castillo-Martínez, E., Williams, A. J. & Attfield, J. P. (2006). *J. Solid State Chem.* **179**, 3505–3510.
Chen, W.-T., Wang, C.-W., Wu, H.-C., Chou, F.-C., Yang, H.-D., Simonov, A. & Senn, M. S. (2018). *Phys. Rev. B*, **97**, 144102.
Dzyaloshinsky, I. (1958). *J. Phys. Chem. Solids*, **4**, 241–255.
Fox, D. L., Tilley, D. R., Scott, J. F. & Guggenheim, H. J. (1980). *Phys. Rev. B*, **21**, 2926–2936.
Fukushima, T., Stroppa, A., Picozzi, S. & Perez-Mato, J. M. (2011). *Phys. Chem. Chem. Phys.* **13**, 12186–12190.
Giovannetti, G., Kumar, S., van den Brink, J. & Picozzi, S. (2009). *Phys. Rev. Lett.* **103**, 037601.
Glazer, A. M. (1972). *Acta Cryst.* B**28**, 3384–3392.
Hatch, D. & Stokes, H. (1987). *Phys. Rev. B*, **35**, 8509–8516.
Hatch, D. M. & Stokes, H. T. (2003). *J. Appl. Cryst.* **36**, 951–952.
Hatch, D. M., Stokes, H. T., Aleksandrov, K. S. & Misyul, S. V. (1989). *Phys. Rev. B*, **39**, 9282–9288.

Howard, C. J. & Carpenter, M. A. (2010). *Acta Cryst.* B**66**, 40–50.

Howard, C. J. & Stokes, H. T. (1998). *Acta Cryst.* B**54**, 782–789.

Howard, C. J. & Stokes, H. T. (2005). *Acta Cryst.* A**61**, 93–111.

Karen, P., Woodward, P. M., Lindén, J., Vogt, T., Studer, A. & Fischer, P. (2001). *Phys. Rev. B*, **64**, 214405.

Khalyavin, D. D., Salak, A. N., Manuel, P., Olekhnovich, N. M., Pushkarev, A. V., Radysh, Y. V., Fedorchenko, A. V., Fertman, E. L., Desnenko, V. A. & Ferreira, M. G. S. (2015). *Z. Kristallogr.* **230**, 767–774.

King, G. & Woodward, P. M. (2010). *J. Mater. Chem.* **20**, 5785.

Knight, K. S. (2009). *Can. Mineral.* **47**, 381–400.

Kovalev, O. V. (1993). *Representations of the Crystallographic Space Groups: Irreducible Representations, Induced Representations, and Corepresentations.* Philadelphia: Gordon and Breach Science.

Kresse, G. & Furthmüller, J. (1996). *Comput. Mater. Sci.* **6**, 15–50.

Kresse, G. & Hafner, J. (1993). *Phys. Rev. B*, **47**, 558–561.

Levanyuk, A. P. & Sannikov, D. G. (1974). *Sov. Phys. Usp.* **17**, 199–214.

Liechtenstein, A., Anisimov, V. & Zaanen, J. (1995). *Phys. Rev. B*, **52**, R5467–R5470.

Markkula, M., Arevalo-Lopez, A. M., Kusmartseva, A., Rodgers, J. A., Ritter, C., Wu, H. & Atteld, J. P. (2011). *Phys. Rev. B*, **84**, 1–5.

Miller, S. C. & Love, W. F. (1967). *Tables of Irreducible Representations of Space Groups and Co-Representations of Magnetic Space Groups.* Boulder: Pruett.

Moriya, T. (1960). *Phys. Rev.* **120**, 91–98.

Mulder, A. T., Benedek, N. A., Rondinelli, J. M. & Fennie, C. J. (2013). *Adv. Funct. Mater.* **23**, 4810–4820.

Orobengoa, D., Capillas, C., Aroyo, M. I. & Perez-Mato, J. M. (2009). *J. Appl. Cryst.* **42**, 820–833.

Perdew, J. P., Ruzsinszky, A., Csonka, G. I., Vydrov, O. A., Scuseria, G. E., Constantin, L. A., Zhou, X. & Burke, K. (2008). *Phys. Rev. Lett.* **100**, 136406.

Perez-Mato, J. M., Orobengoa, D. & Aroyo, M. I. (2010). *Acta Cryst.* A**66**, 558–590.

Perez-Mato, J. M., Ribeiro, J. L., Petricek, V. & Aroyo, M. I. (2012). *J. Phys. Condens. Matter*, **24**, 163201.

Rodriguez, E. E., Proffen, Th., Llobet, A., Rhyne, J. J. & Mitchell, J. F. (2005). *Phys. Rev. B*, **71**, 104430.

Rondinelli, J. M. & Fennie, C. J. (2012). *Adv. Mater.* **24**, 1961–1968.

Saxena, A., Barsch, G. R. & Hatch, D. M. (1994). *Phase Transitions*, **46**, 89–142.

Stokes, H. T. & Campbell, B. J. (2017). *Acta Cryst.* A**73**, 4–13.

Stokes, H. T., Campbell, B. J. & Cordes, R. (2013). *Acta Cryst.* A**69**, 388–395.

Stokes, H. T. & Hatch, D. M. (1988). *Isotropy Subgroups of the 230 Crystallographic Space Groups.* Singapore: World Scientific.

Stokes, H. T. & Hatch, D. M. (1991). *Phase Transitions*, **34**, 53–67.

Stokes, H. T., Kisi, E. H., Hatch, D. M. & Howard, C. J. (2002). *Acta Cryst.* B**58**, 934–938.

Talanov, M. V., Shirokov, V. B. & Talanov, V. M. (2016). *Acta Cryst.* A**72**, 222–235.

Tokunaga, Y., Furukawa, N., Sakai, H., Taguchi, Y., Arima, T. H. & Tokura, Y. (2009). *Nat. Mater.* **8**, 558–562.

Varignon, J., Bristowe, N. C., Bousquet, E. & Ghosez, P. (2015a). *Sci. Rep.* **5**, 15364.

Varignon, J., Bristowe, N. C., Bousquet, E. & Ghosez, P. (2015b). *C. R. Phys.* **16**, 153–167.

Varignon, J., Bristowe, N. C. & Ghosez, P. (2016). *Phys. Rev. Lett.* **116**, 057602.

Vogt, T., Woodward, P. M., Karen, P., Hunter, B. A., Henning, P. & Moodenbaugh, A. R. (2000). *Phys. Rev. Lett.* **84**, 2969–2972.

Wang, X. *et al.* (2015). *Phys. Rev. Lett.* **115**, 087601.

Yamauchi, K. (2013). *J. Phys. Soc. Jpn*, **82**, 043702.

Yang, Y., Iñiguez, J., Mao, A. J. & Bellaiche, L. (2014). *Phys. Rev. Lett.* **112**, 057202.

Yang, M., Oró-Solé, J., Rodgers, J. A., Jorge, A. B., Fuertes, A. & Attfield, J. P. (2011). *Nat. Chem.* **3**, 47–52.

Yang, Y., Ren, W., Stengel, M., Yan, X. H. & Bellaiche, L. (2012). *Phys. Rev. Lett.* **109**, 057602.

Young, J. & Rondinelli, J. M. (2013). *Chem. Mater.* **25**, 4545–4550.

Young, J., Stroppa, A., Picozzi, S. & Rondinelli, J. M. (2015). *J. Phys. Condens. Matter*, **27**, 283202.

Zhao, H. J., Bellaiche, L., Chen, X. M. & Iñiguez, J. (2017). *Nat. Commun.* **8**, 14025.

Zhou, Q. & Rabe, K. M. (2013). *arXiv*:1306.1839.

Zuo, P., Colin, C. V., Klein, H., Bordet, P., Suard, E., Elkaim, E. & Darie, C. (2017). *Inorg. Chem.* **56**, 8478–8489.